



Effect of H₂S on the CO₂ corrosion of carbon steel in acidic solutions

Yoon-Seok Choi^{a,*}, Srdjan Nesic^a, Shiun Ling^b

^a Institute for Corrosion and Multiphase Technology, Department of Chemical and Biomolecular Engineering, Ohio University, 342 West State Street, Athens, OH 45701, USA

^b ExxonMobil Research and Engineering Company, 1545 Route 22 East, Annandale, NJ 08801, USA

ARTICLE INFO

Article history:

Received 30 June 2010

Received in revised form 13 August 2010

Accepted 14 August 2010

Available online 20 August 2010

Keywords:

CO₂/H₂S corrosion

Carbon steel

Iron sulfide

Acid solutions

Precipitation

ABSTRACT

The objective of this study is to evaluate the effect of low-level hydrogen sulfide (H₂S) on carbon dioxide (CO₂) corrosion of carbon steel in acidic solutions, and to investigate the mechanism of iron sulfide scale formation in CO₂/H₂S environments. Corrosion tests were conducted using 1018 carbon steel in 1 wt.% NaCl solution (25 °C) at pH of 3 and 4, and under atmospheric pressure. The test solution was saturated with flowing gases that change with increasing time from CO₂ (stage 1) to CO₂/100 ppm H₂S (stage 2) and back to CO₂ (stage 3). Corrosion rate and behavior were investigated using linear polarization resistance (LPR) technique. Electrochemical impedance spectroscopy (EIS) and potentiodynamic tests were performed at the end of each stage. The morphology and compositions of surface corrosion products were analyzed using scanning electron microscopy (SEM)/energy dispersive spectroscopy (EDS) and X-ray photoelectron spectroscopy (XPS). The results showed that the addition of 100 ppm H₂S to CO₂ induced rapid reduction in the corrosion rate at both pHs 3 and 4. This H₂S inhibition effect is attributed to the formation of thin FeS film (tarnish) on the steel surface that suppressed the anodic dissolution reaction. The study results suggested that the precipitation of iron sulfide as well as iron carbonate film is possible in the acidic solutions due to the local supersaturation in regions immediately above the steel surface, and these films provide corrosion protection in the acidic solutions.

© 2010 Elsevier Ltd. All rights reserved.

1. Introduction

The number of sour (CO₂ + H₂S containing) oil and gas fields being produced worldwide is increasing, as sweet (CO₂ containing) fields are being depleted, and higher oil prices made it possible for profitable development of sour oil and gas fields. A concern in the production and transportation sour oil and gas is the corrosion caused by the acid gases CO₂ and H₂S. Even though corrosion resistant alloys (CRA) has long been available as a material selection option that mitigates CO₂ and H₂S corrosion, carbon steel is in general more cost-effective for oil and gas facilities and hence, is the most widely used material option [1]. The internal corrosion of carbon steel pipeline in the presence of CO₂ and H₂S was firstly recognized in the 1940s and has been investigated for over 60 years [2].

Several studies have shown that the presence of H₂S could either cause an acceleration or an inhibition of the corrosion of carbon steel, depending on the partial pressure of H₂S. It was reported from early studies that at H₂S concentrations below 690 Pa, a protective iron sulfide film formed. At H₂S concentrations greater than 690 Pa, a non-protective film formed [3–5]. More recently, Ma et al.

claimed that H₂S provides a strong inhibition under certain special conditions that have lower H₂S concentration (≤ 0.04 mmol dm⁻³), pH value of 3–5, and longer immersion time (≥ 2 h) [6]. Abelev et al. also reported that 5 ppm of H₂S concentration have an inhibiting effect on corrosion in the presence of CO₂ [7]. Even though there is no absolute criterion for the H₂S concentration that provides inhibition, it has been suggested that the inhibition effect is related to the formation of iron sulfide with different crystal structures, such as amorphous ferrous sulfide, mackinawite, cubic ferrous sulfide, smythite, greigite, pyrrhotite, troilite, and pyrite [8–12].

However, there is no clear understanding of the nature of the surface layer formed in CO₂/H₂S environments as well as their protective properties in acidic solutions when the concentration of H₂S is too low to cause a concern of the surface layer cracking or blistering. The objective of this study is to evaluate the effect of very low-level H₂S on CO₂ corrosion of carbon steel in acidic solutions, and to investigate the mechanism of the iron sulfide layer formation in CO₂/H₂S environments.

2. Experimental

The specimens were made of carbon steel (AISI C1018) that has a chemical composition of 0.21% C, 0.05% Mn, 0.09% P, 0.05% S, 0.38% Si and balance Fe. The specimen shape was of a cylindrical geometry, 1.3 cm in diameter and 1.3 cm in height, and would have its

* Corresponding author. Tel.: +1 740 593 9944.

E-mail address: choiy@ohio.edu (Y.-S. Choi).

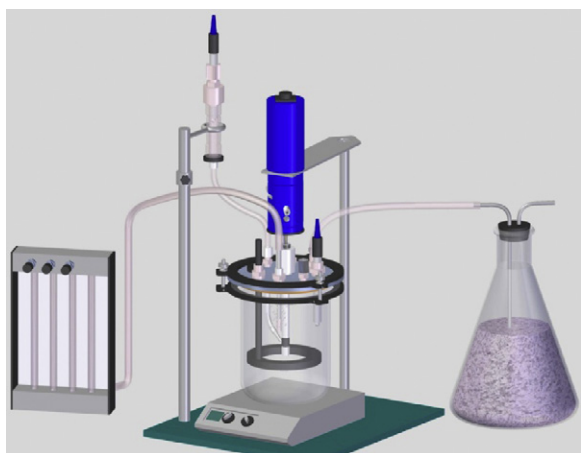


Fig. 1. Schematics of the test apparatus.

outer surface exposed to solution during testing. The specimen surface was grounded to a 600 grit finish using silicon carbide paper, then cleaned with isopropyl alcohol in an ultrasonic bath and dried.

The corrosion tests were carried out in a 2 L glass cell which contained a rotating cylinder working electrode, a reference electrode consisted of a glass capillary probe connected to a saturated Ag/AgCl electrode, and a platinum wire counter electrode. The schematic of this experimental setup is shown in Fig. 1. All the tests were conducted in 1 wt.% NaCl solutions at room temperature and atmospheric pressure. Gas mass-flow controllers were used to control the flow rates of CO₂ and H₂S to the test cell, as well as to obtain the desired H₂S concentration. These gases were mixed by flowing through a mixer before injecting into the test cell. Before specimen was inserted into the solution, the solution was purged with CO₂ for 2 h in order to deoxygenate, then with pH adjusted to the desired value by adding a deoxygenated HCl solution or NaHCO₃ solution as appropriate.

Table 1 shows the test conditions, and Fig. 2 shows the experimental procedures. This test procedure was designed to investigate the effect of H₂S on the corrosion of carbon steel in CO₂ environments; the environment was changed from CO₂ (stage 1) to CO₂/100 ppm H₂S (stage 2) and then back to CO₂ (stage 3). During experiment, instantaneous corrosion rates were monitored with linear polarization resistance (LPR) measurements made at regular time intervals. Using the polarization resistance (R_p) obtained from LPR measurements, the corrosion current density (j_{corr}) was calculated using Eq. (1) [13], and the resulting j_{corr} yields the corrosion rate using Eq. (2) [14]:

$$j_{\text{corr}} = \frac{B}{R_p} = \frac{\beta_a \times \beta_c}{2.3 \times R_p \times (\beta_a + \beta_c)} \quad (1)$$

$$\text{corrosion rate (mm/year)} = \frac{0.00327 \times j_{\text{corr}} (\mu\text{A}/\text{cm}^2) \times \text{EW}}{\text{density (g}/\text{cm}^3)} \quad (2)$$

Table 1
Test conditions.

Parameter	Description
Material	C1018 carbon steel
Rotation speed	1000 rpm
Solution	Deionized water with 1 wt.% NaCl
Temperature	25 °C
Total pressure	0.1 MPa
CO ₂ partial pressure	0.097 MPa
H ₂ S concentration	100 ppm (0.01 kPa)
pH	3, 4

where β_a is the anodic Tafel constant, β_c is the cathodic Tafel constant, 0.00327 is a constant factor used for dimension and time conversion factor, and EW is the equivalent weight in grams. In the present study, different B values were applied to each stage. For CO₂ environments (stages 1 and 3), 0.026 V was used as B value, whereas 0.013 V was used for CO₂/H₂S environment (stage 2).

The experimental procedures shown in Fig. 2 were to have electrochemical impedance spectroscopy (EIS) measurements and potentiodynamic scan performed at the end of each stage. There was, however, the concern that the potentiodynamic scan may cause irreversible alterations to the sample surface (especially the anodic scan) which could render the subsequent testing questionable. Consequently, the actual study consisted of three separate tests; each had only one potentiodynamic scan performed at the very end of the test. In other words, each of these tests had started from the very beginning shown in Fig. 2, and had run to the end of stages 1, 2 and 3, respectively, when a potentiodynamic scan was performed that concluded the respective test.

LPR measurements were performed in a range of ± 10 mV with respect to the corrosion potential, and a scan rate of 0.166 mV/s. EIS measurements were conducted in the frequency range from 10 kHz and 10 mHz, with an AC signal amplitude of 10 mV (rms) at the corrosion potential. The potentiodynamic scans were carried out after the completion of the EIS measurements, and was conducted in the following manner. The scan was first conducted in the cathodic direction from the open-circuit potential (OCP) to -1.2 V vs. sat. Ag/AgCl, with a scan rate of 0.166 mV/s. The OCP was then allowed to return to its previous value, which would occur within about 20 min. Then the scan was conducted in the anodic direction from OCP to -0.4 V vs. sat. Ag/AgCl, with a scan rate of 0.166 mV/s.

After the experiment, the specimen was used for additional ex situ analyses. The morphology and compositions of corrosion products from each stage were analyzed with scanning electron microscopy (SEM), energy dispersive X-ray spectroscopy (EDS) and X-ray photoelectron spectroscopy (XPS).

3. Results

3.1. Effect of H₂S addition/removal in CO₂ environment at pH 4

The results of OCP and LPR measurements at pH 4 are summarized in Fig. 3. At the transition from stage 1 to stage 2, when 100 ppm H₂S was added into the CO₂ environment, the OCP increased and the corrosion rate decreased immediately. This phenomenon is probably related to the formation of protective iron sulfide film on the steel surface. At the end of stage 3, at which point H₂S was completely removed from the CO₂ environment, the OCP and the corrosion rate returned their previous levels in stage 1, which suggest the dissolution of the iron sulfide film and re-exposure of the bare steel surface to the environment.

Fig. 4 shows the Nyquist plots measured at the end of each stage. All impedance spectra showed a depressed capacitive loop at high frequencies indicating a double-layer capacitance, as well as an inductive loop at low frequencies. Depressed semi-circles are not uncommon for iron dissolution in acidic media and it had been suggested in the literature that this behavior might be related to a heterogeneous surface roughness and the nonuniform distribution of current density on the surface [15,16]. In addition, no mass transfer controlled impedance was observed under these conditions. However, it was not a pure charge transfer controlled process either because the inductive loop at low frequencies [17] indicated that the iron dissolution mechanism might occur in two or more steps involving an adsorbed intermediate [18,19]. As Fig. 4 shows, the diameter of the semi-circle increased with the addition of H₂S indicating a decreased corrosion rate, which suggests

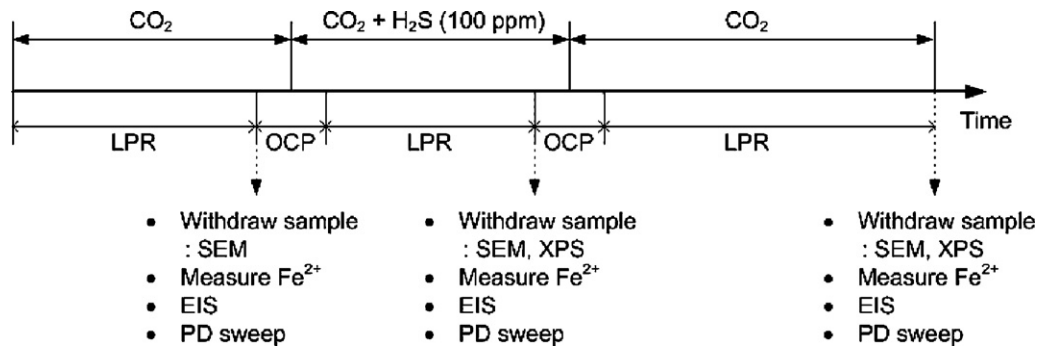


Fig. 2. Experimental procedure for electrochemical corrosion study in pHs 3 and 4.

the H₂S induced inhibition against the CO₂ corrosion of carbon steel. When H₂S was removed from the system, the diameter of the semi-circle decreased indicating an increased corrosion rate, which is consistent with the occurrence of the dissolution of iron sulfide film. It is further noted that the shape of these Nyquist plots (capacitive loop + inductive loop) did not change with the addition and removal of H₂S, indicating the same mechanism for the steel corrosion throughout the entire test, from stage 1 to stage 3.

The polarization curves of carbon steel obtained at the end of each stage at pH 4 were also consistent with the understanding that the inhibition effect of H₂S on CO₂ corrosion of carbon steel was due to the formation of a protective film of iron sulfides (Fig. 5). As can be seen in Fig. 5, the addition of H₂S reduced the anodic current from the iron dissolution reaction, whereas, the cathodic current and hence the cathodic reactions were much less affected. This observation is consistent with existing understanding that many types of iron sulfides are electronic conductors [20], and hence a surface coverage of iron sulfide film may impede the movement of dissolved iron through the film, but not the movement of electrons through the film to continue the cathodic reactions. Comparing the curves from stage 1 and stage 2 in Fig. 5, it can be seen that the OCP increase and corrosion rate decrease in the stage 2 curve (also shown in Fig. 3) were mostly the results of a change in the anodic curve. Comparing the anodic polarization curves from stage 2 and stage 3, it is suggested that in stage 2 environment with protective film formed by H₂S addition, the film is sufficiently stage to inhibit the anodic dissolution reaction at the lower anodic overpotential, but may be damaged by higher overpotential resulting in the stage 2 anodic curve to eventually approach that of stage 3 one at high overpotential.

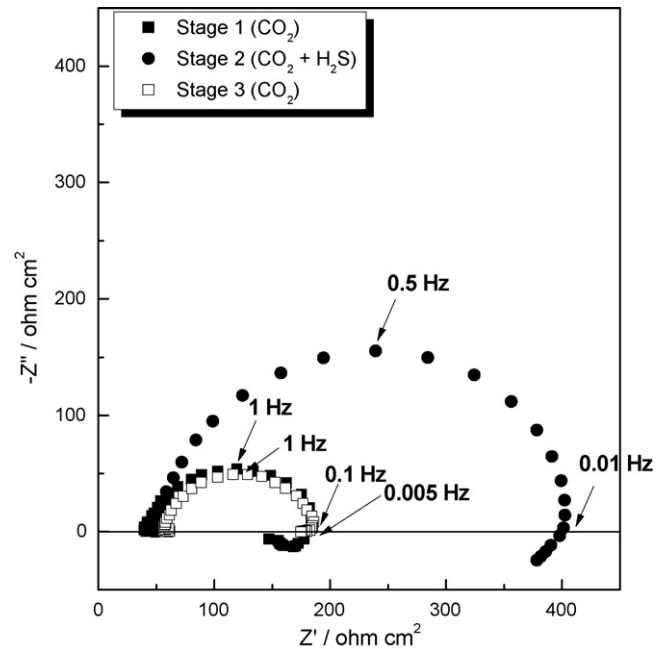


Fig. 4. Nyquist plots of carbon steel tested at pH 4, taken at the end of each stage.

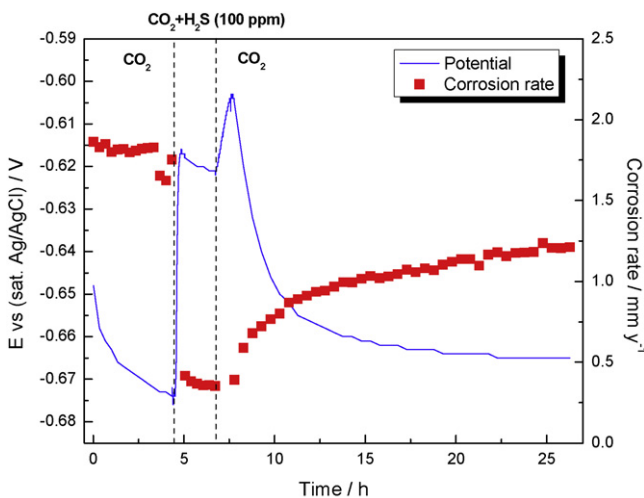


Fig. 3. OCP and corrosion rate of carbon steel tested at pH 4.

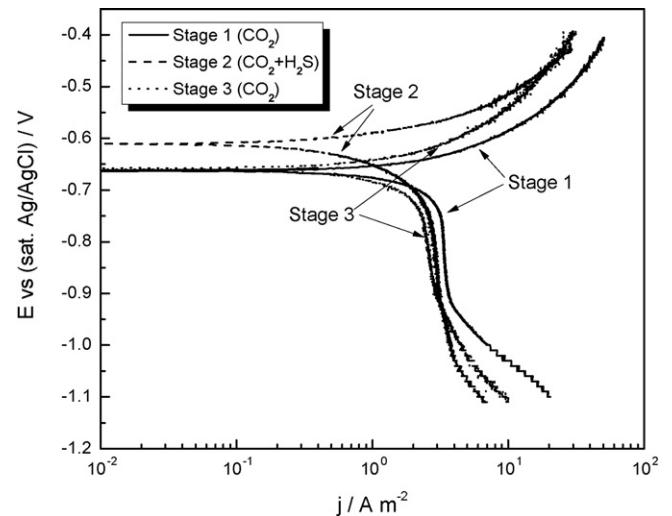


Fig. 5. Polarization curves of carbon steel tested at pH 4, taken at the end of each stage.

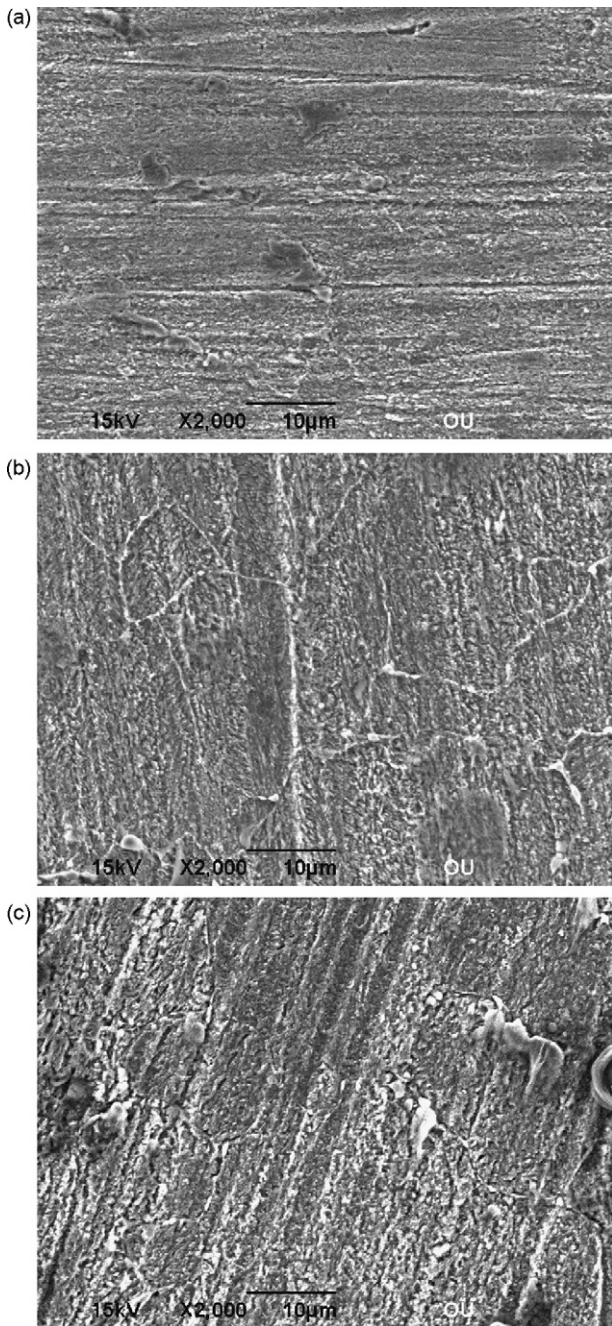


Fig. 6. SEM surface morphologies of carbon steel tested at pH 4, at the end of: (a) stage 1 (CO₂), (b) stage 2 (CO₂/H₂S), (c) stage 3 (CO₂).

The SEM morphologies of the surface of steel specimens collected at the end of each stage are shown in Fig. 6. No significant difference was observed in the surface morphology from stage 1 to stage 3, which all showed indications that the active dissolution of iron was occurring from within the grains. In addition, EDS analysis showed that only Fe and C were detected on these steel surface (the EDS spectra are not shown).

3.2. Effect of H₂S addition/removal in CO₂ environment at pH 3

Fig. 7 summarized the results of OCP and LPR measurements at pH 3. Here the corrosion rate showed immediate decrease at the addition of 100 ppm H₂S into the CO₂ environment, followed by further, gradual decreasing throughout stage 2. This corrosion

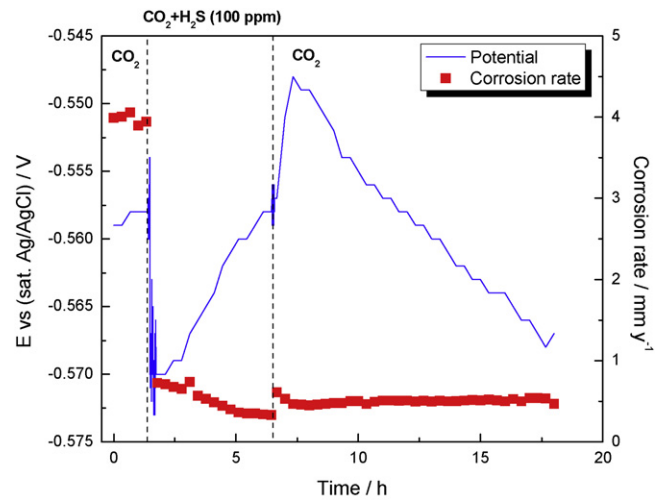


Fig. 7. OCP and corrosion rate of carbon steel tested at pH 3.

rate behavior is similar to that previously observed at pH 4. The OCP, however, followed a very different trend from that observed at pH 4. It decreased immediately at the addition of H₂S, followed by gradual increasing throughout stage 2. It is noted that, in stage 2, the gradual increase of OCP coupled with a gradual decrease of corrosion rate is may be explained by the notion of an inhibition of the anodic dissolution reaction by the formation of an iron sulfide film.

Examining stages 3 in Figs. 3 and 7, it is interesting to note that the trend of corrosion rate after removing H₂S from the environments was different between these two cases at pH 3 and 4, respectively. Here, at pH 3, the corrosion rate did not increase to restore itself to a level similar to the previous stage 1. Instead, it further decreased slightly, and then remained at a low but constant value throughout the remainder of the test, even though in the same time period the OCP was decreasing continuously with time.

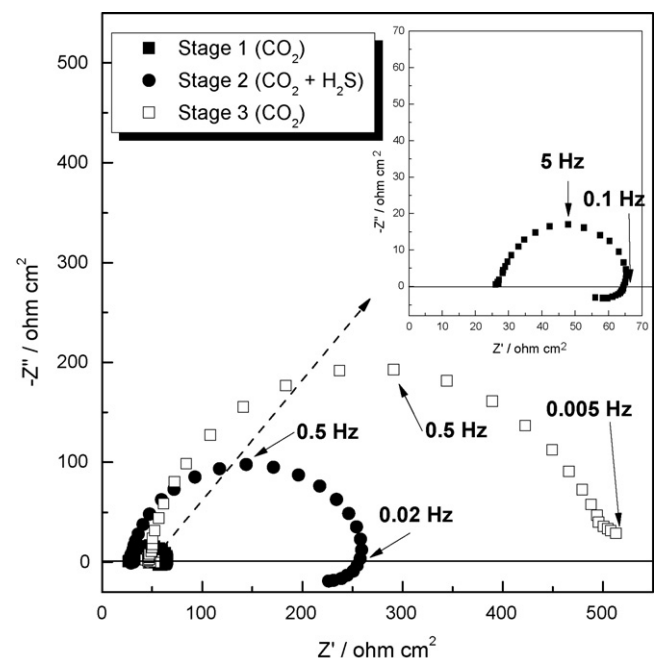


Fig. 8. Nyquist plots of carbon steel tested at pH 3, taken at the end of each stage.

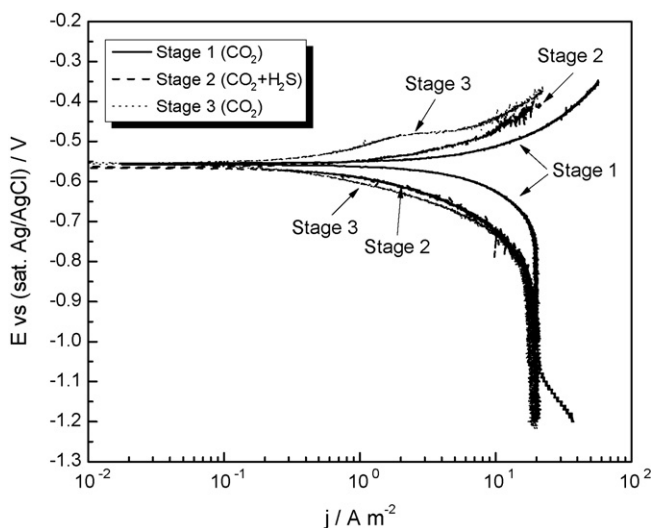


Fig. 9. Polarization curves of carbon steel tested at pH 3 taken at the end of each stage.

Fig. 8 shows the Nyquist plots measured at the end of each stage. The impedance spectra at end of stage 1 and stage 2 showed a depressed capacitive loop at high frequencies as well as an inductive loop at low frequencies, whereas that at end of stage 3 showed the capacitive loop without the inductive loop. This indicates that the corrosion mechanism in stage 3 is different from that in stage 1 and stage 2. In addition, as can be seen in Fig. 8, the diameter of the Nyquist plot increased with the addition of H_2S , which implies corrosion inhibition due to the formation of iron sulfide on the steel surface similar to that observed in the test at pH 4. The Nyquist plot diameter, however, further increased in stage 3 even though H_2S was removed from the system. This observation suggested a further increase of corrosion inhibition into stage 3, but it was unclear whether the inhibition was on the anodic or cathodic reactions.

Fig. 9 shows the polarization curves measured at the end of each stage in the test at pH 3. By comparing the stage 1 and stage 2 polarization curves, it can be seen that the addition of H_2S suppressed the anodic reactions, and suppressed the cathodic reactions in the lower overpotential ranges. In stage 3, when H_2S was removed from the system, the anodic current was further reduced, whereas the cathodic current was not affected. This implies that the increase in the diameter of Nyquist plot at stage 3 is related to the inhibition of the anodic reaction. In addition, this reduction in the anodic reaction is only effective at the lower overpotential range, indicating the formation of protective layer even at stage 3.

Fig. 10 shows the SEM observed morphologies of the steel surface at the end of each stage. No significant difference was observed in these the corroded surfaces, similar to that found in the case of pH 4 test. Additionally, EDS analysis found that only Fe and C were detected on these steel surfaces from the EDS analysis (the EDS spectra are not shown).

4. Discussion

Fig. 11 shows a comparison of carbon steel corrosion rates measured at the end of each stage in pHs 3 and 4 conditions. At pH 4, it can be seen from Fig. 11 that the addition of low concentration of H_2S (100 ppm) into the CO_2 environment reduced the corrosion rate, but this inhibition effect disappeared when H_2S was removed from the system. However, at pH 3, while the addition of low concentration H_2S also had inhibition effect, the reduced corrosion rate remained low even in stage 3, after the removal of H_2S from the system. This last observation was unexpected because the solubil-

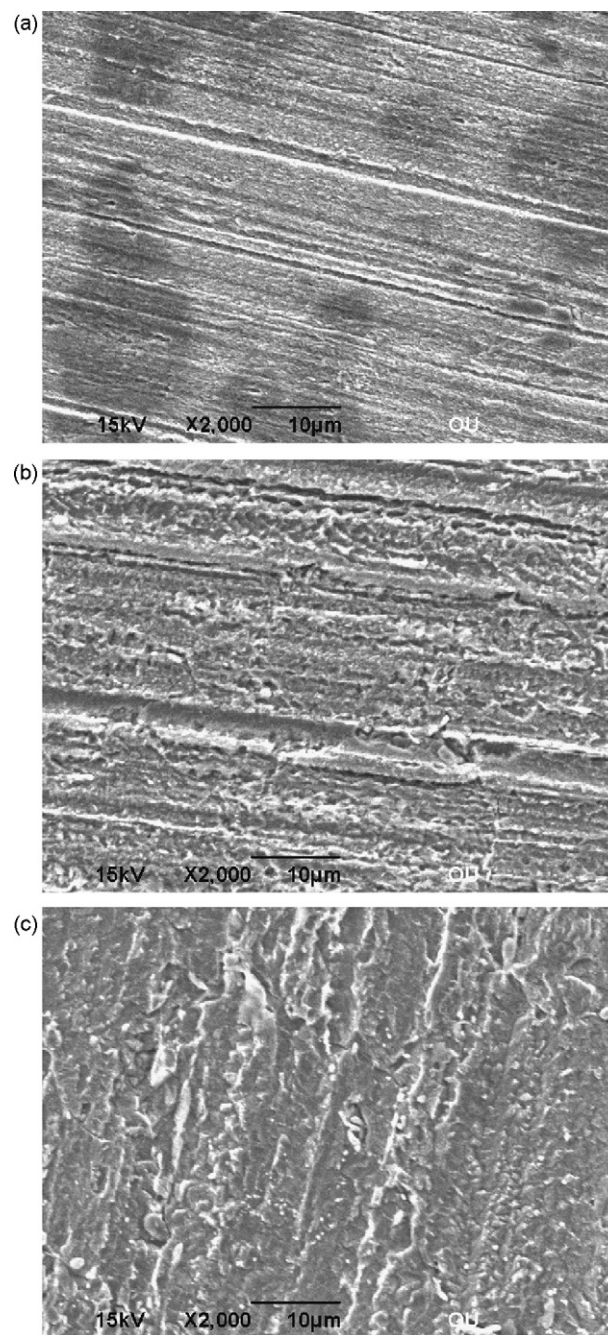


Fig. 10. SEM surface morphologies of carbon steel tested at pH 3, at the end of: (a) stage 1 (CO_2), (b) stage 2 (CO_2/H_2S), (c) stage 3 (CO_2).

ities of iron sulfide and iron carbonate increase with decreasing pH [21].

In order to better investigate this phenomenon, an additional experiment was performed at pH 3. Fig. 12 shows the test procedure, which was similar to the previous experiment procedure shown in Fig. 2, except here it skipped stage 1 and started from stage 2. The resulting OCP and LPR measurements at pH 3 are presented in Fig. 13. It was observed that the variation in OCP with increasing time in stage 2 and stage 3 showed the same trend as that in stage 2 and stage 3 in the previous test (Fig. 7). The variation in corrosion rate, however, was found to be different from that in the previous test. The corrosion rate was found to increase in stage 3, after the removal of H_2S from the system. Fig. 14 shows the Nyquist plots measured at the end of each stage. The impedance

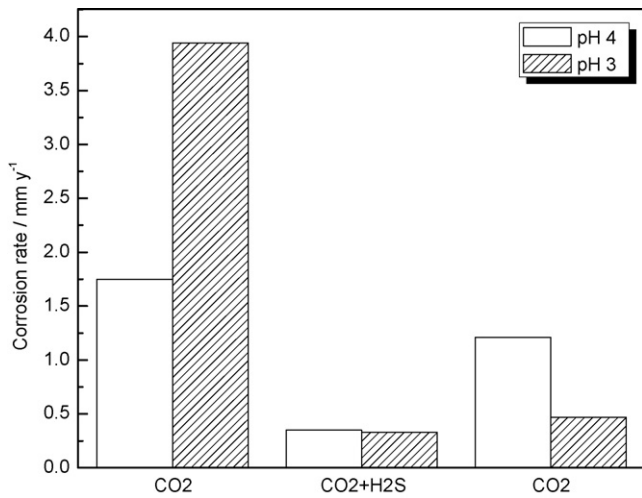


Fig. 11. Carbon steel corrosion rates measured at the end of each stage in pHs 3 and 4 conditions.

spectra measured at stage 2 showed a depressed capacitive loop at high frequencies and an inductive loop at low frequencies. At stage 3, the impedance spectra showed two capacitive loops at both high and low frequencies, whereas the low frequency inductive loop had disappeared. The diameter of Nyquist plot decreased with the removal of H₂S, which implies the loss of inhibition on the steel surface due to dissolution of iron sulfide, similar to the case in pH 4. Fig. 15 compares the polarization curves obtained at end of stage 3 from the two pH 3 tests that was, respectively, with and without stage 1 exposure. It can be seen that when the specimen had gone through stage 1 exposure, there was more reduction in the anodic

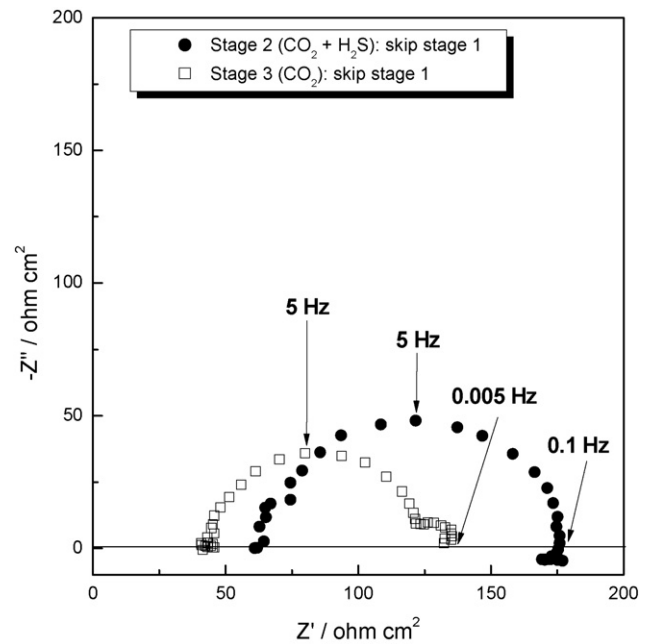


Fig. 14. Nyquist plots of carbon steel tested at pH 3 at the end of each stage (skip stage 1).

reaction in stage 3. This implies that pre-corrosion of carbon steel in the stage 1 promotes the formation of more stable iron sulfide in stage 2, and even provides more protection in stage 3 possibly by the additional formation of iron carbonate as well. However, the detailed mechanism for the effect of pre-corrosion in CO₂ environment (stage 1) is not understood, and further investigations are needed.

As shown in Figs. 3 and 7, the addition of 100 ppm H₂S to CO₂ environment at pHs 3 and 4 caused a very fast response in the OCP and a sharp reduction of carbon steel corrosion rate. All the above mentioned observations and the associated discussions indicated that the addition of low H₂S concentration induced the formation of protective iron sulfide film on the steel surface. In addition, the films that caused these large changes in the electrochemical kinetics were thin and not observable in either SEM nor EDS [20].

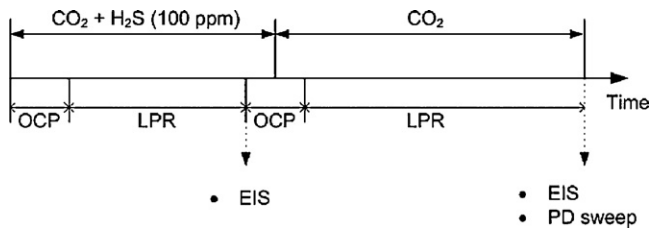


Fig. 12. Experimental procedure for electrochemical corrosion study in pH 3 without stage 1.

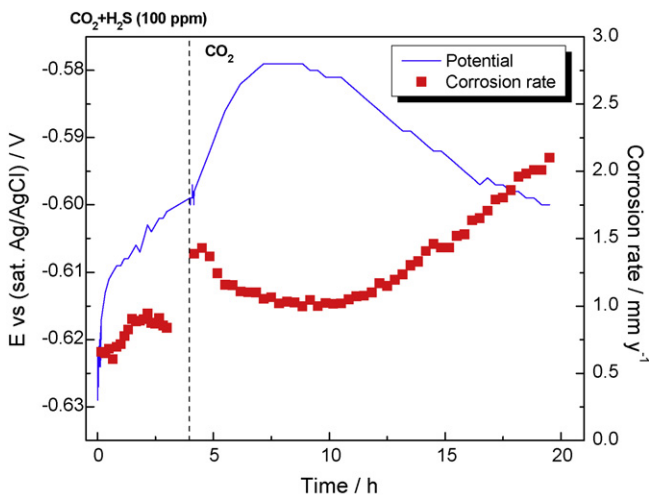


Fig. 13. OCP and corrosion rate of carbon steel tested in pH 3. This test procedure skipped stage 1.

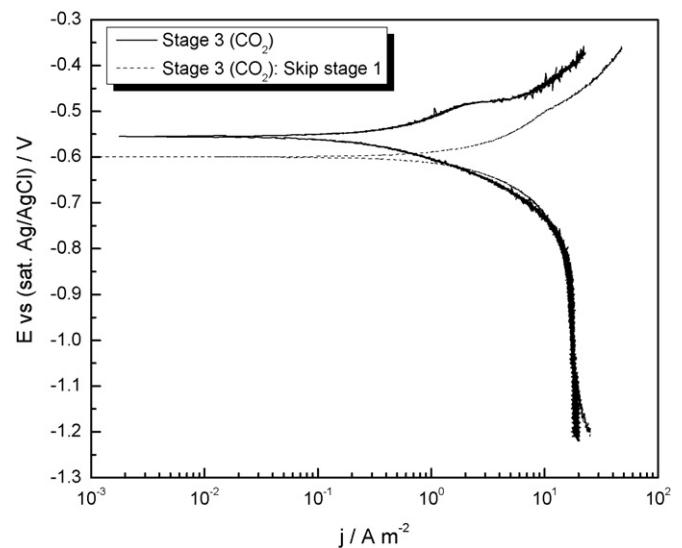


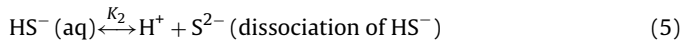
Fig. 15. Polarization curves of carbon steel in pH 3 at stage 3 with and without stage 1.

Although there have been a number of researchers investigated the mechanisms of iron sulfide formation, the actual mechanism of iron sulfide formation in H_2S environment is nevertheless still unclear, and it is still unclear whether the iron sulfide is formed by direct solid state reaction or precipitation or both. In the present study, the thermodynamics of iron sulfide formation were evaluated in order to understand the mechanism and kinetics of iron sulfide formation in the acidic solutions.

When H_2S dissolves into a water solution, the vapor–liquid equilibrium of H_2S is described as:



Upon dissolution, the dissolved H_2S (aq) is involved in a sequence of chemical reactions as follows:



The concentrations of these sulfide species have been studied by a number of researchers using either experiments or theoretical thermodynamic models [22].

If reaction (4) or (5) continues together with an increasing in concentration of Fe^{2+} , a condition of supersaturation of mackinawite at the steel surface may be achieved, which led to the nucleation and growth of mackinawite on the steel surface may occur via a precipitation mechanism. In the present study, in order to calculate the degree of saturation of mackinawite, “[HS^-] based expressions” were used instead of “[S^{2-}] based expressions” because of the prediction of S^{2-} concentration tends to be inaccurate [23]. The equation used to calculate the degree of saturation of mackinawite (SS) is shown in the following:

$$SS = \frac{[Fe^{2+}][HS^-]/[H^+]}{K_{sp,mack}} \quad (6)$$

where $[Fe^{2+}]$, $[HS^-]$ and $[H^+]$ are the concentrations (mol/L) of ferrous ion, bisulfide ion, and hydrogen ion, respectively. $K_{sp,mack}$ is the equilibrium solubility product of mackinawite.

The film precipitation will occur when the SS value exceeds unity, i.e. when the solution is saturated. The saturation degree of mackinawite depends on the solubility limit of mackinawite in the water solution. The solubility product of mackinawite ($K_{sp,mack}$) at different temperatures had been expressed as follows [23]:

$$K_{sp,mack} = 10^{(2848.779/T_k) - 6.347 + \log(K_1)} \quad (7)$$

where T_k is the absolute temperature (in Kelvin) and K_1 is the first dissociation constant of H_2S (in mol/L) of reaction (4).

The degree of saturation for mackinawite at 25 °C had been calculated at different pH values, and the results are plotted against Fe^{2+} concentration as shown in Fig. 16. In addition, the concentrations of Fe^{2+} in the solution measured at the end of each stage for the tests at bulk pH of 3 and 4, respectively, were also shown in Fig. 17. As can be seen in Fig. 17, all these Fe^{2+} concentration values remained within the range of 6–11 ppm. From Fig. 16, it can be seen that, with the Fe^{2+} concentrations shown in Fig. 17, at the tests at pHs 3 and 4 would have solution that was under-saturated with respect to mackinawite, and could not achieve saturation until pH becomes higher than 6. This suggests that it is impossible to form mackinawite by precipitation out of bulk solution at pHs 3 and 4 conditions. However, recent research in our lab on CO_2 corrosion has shown that, the pH measured near the surface of corroding carbon steel is higher than the bulk solution pH, in spite of the fact that CO_2 has a good buffering capacity [24]. Fig. 18 presents a comparison of pH values at 25 °C in CO_2 environments, between the bulk solution versus that in near surface region over corroding steel [24]. For the current pHs 3 and 4 corrosion tests in this work,

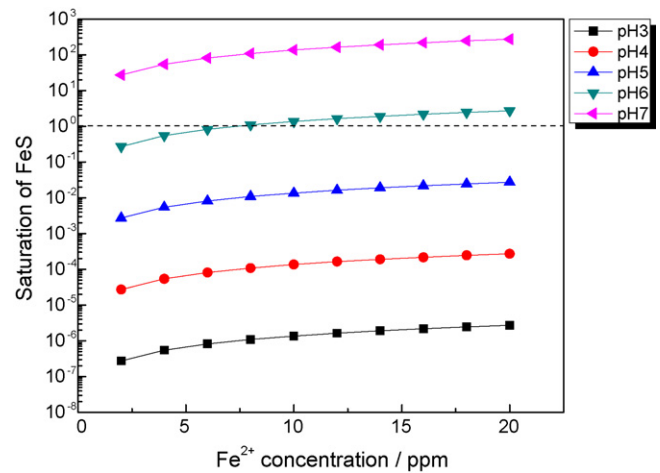


Fig. 16. Calculated degree of saturation for mackinawite at 25 °C and 100 ppm H_2S , plotted for different pH values as a function of Fe^{2+} concentration.

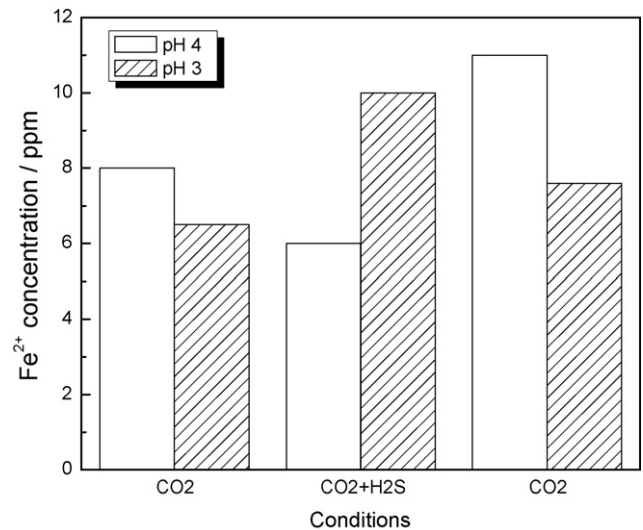


Fig. 17. Ferrous ion concentrations at the end of each stage measured for tests at pHs 3 and 4, respectively.

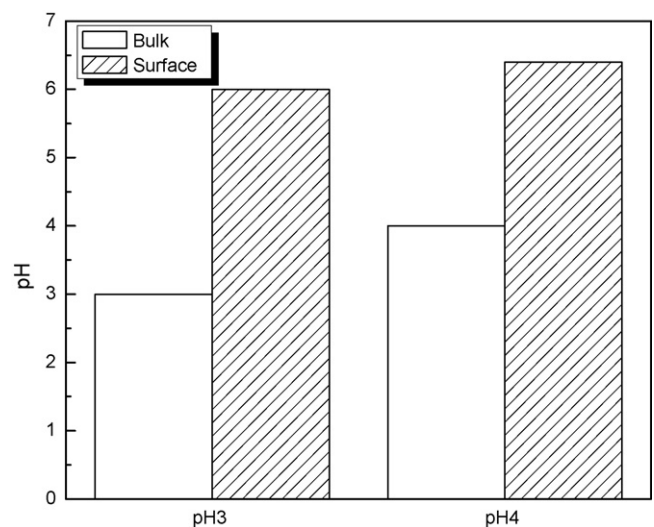


Fig. 18. pH values measured in solution bulk and near surface region of corroding steel (data from Ref. [22]).

Table 2
Solubility limits of iron sulfides and iron carbonate (siderite) at room temperature.

Phase	log(K_{sp}) (mol L ⁻¹) at 25 °C
Amorphous FeS	-2.95
Mackinawite	-3.6
Pyrrhotite	-5.19
Troilite	-5.31
Siderite	-10.89

similar surface pH values (≈ 6) were measured and was found to be higher than the bulk solution pH value. This finding indicates that more alkaline local water chemistry can be present in near surface region during CO₂ corrosion. Thus, immediately over a steel surface undergoing corrosion, it is possible to generate a local alkaline condition that favors the precipitation of iron sulfide or iron carbonate on the steel surface. In order to verify the possibility of precipitation, the degree of saturation of various iron sulfides as well as iron carbonate at 25 °C, pH 6 was calculated, and the results are plotted in Fig. 19 as a function of Fe²⁺ concentration. The solubility limits of iron sulfides and iron carbonate at 25 °C used in the calculation are shown in Table 2 [25,26]. As shown in Fig. 19, the 25 °C, pH 6 solution would be saturated for most of iron sulfides and for iron carbonate. This finding suggests that in an acidic solution, it is possible to have a surface pH that causes local saturation and thus enable the formation of iron sulfides and iron carbonate film on steel sur-

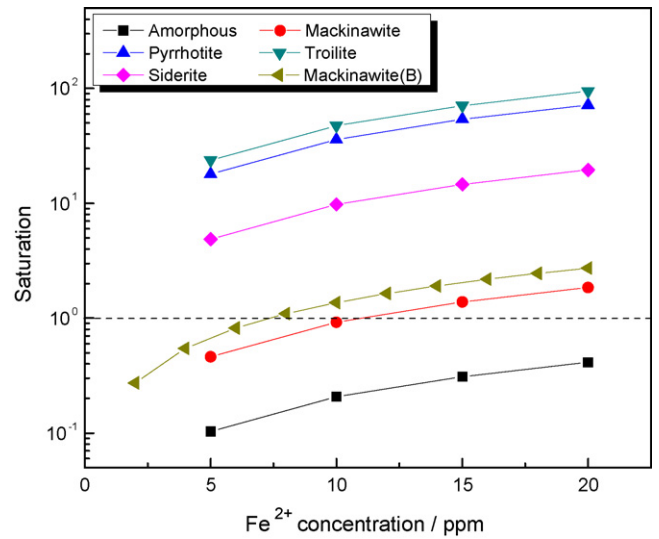


Fig. 19. Calculated degree of saturation for iron sulfides and iron carbonate at 25 °C, 100 ppm H₂S and pH 6, plotted as a function of Fe²⁺ concentration.

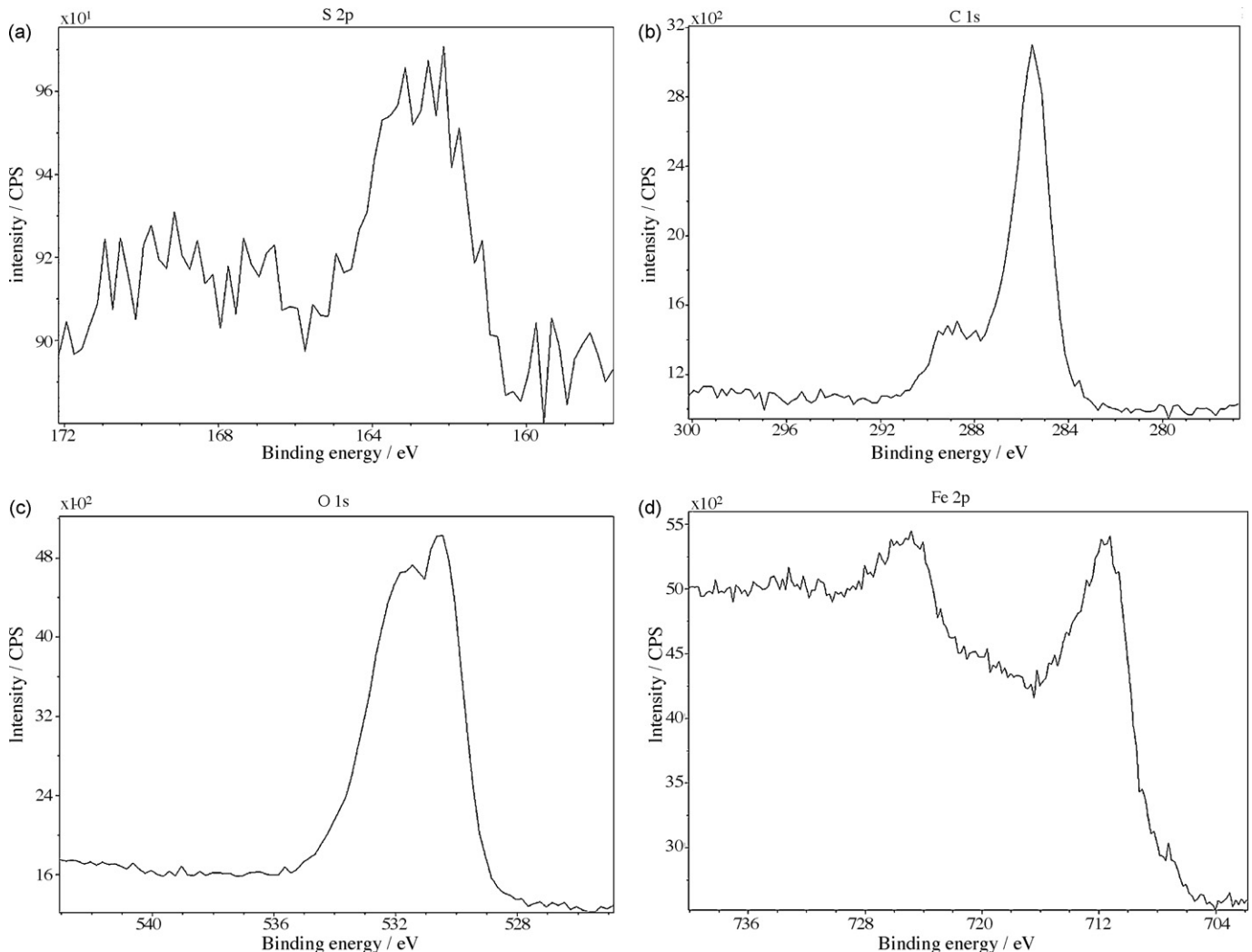


Fig. 20. XPS spectra of carbon steel from pH 3 solution at the end of stage 3: (a) S 2p, (b) C 1s, (c) O 1s, (d) Fe 2p.

face via precipitation. It is further noted that the above discussion indicates that it is also possible for the iron sulfide to form in an acidic solution via the solid state reaction mechanism, because the same favorable alkaline pH in near surface region may also serve to stabilize any surface iron sulfide that might have formed via the solid state mechanisms.

Although the above theoretical calculation demonstrated the possibility of forming iron sulfide in the acidic solutions, in the present study, no sulfur was detected in the EDS analysis. It seems likely that the iron sulfide films formed in stage 2 when H₂S was added were too thin to be detected in SEM and EDS analyses. In order to confirm the presence of iron sulfide on steel surface, XPS analysis was performed on samples that had been exposed to different stages and pHs. As an example, Fig. 20 shows the results of XPS analyses of carbon steel surface from pH 3 solution at the end of stage 3. Similar XPS spectra had been obtained from other samples at the end of stages 2 and 3 in both pHs used. As expected, S 2p_{3/2} peak was found (Fig. 20(a)) and its binding energy is consistent with that of iron sulfide [27]. In addition, C 1s (≈289 eV) and O 1s (≈532 eV) peaks were also detected (Fig. 20(b) and (c)) which were consistent with the presence of iron carbonate [28,29]. The presence of iron sulfide and iron carbonate were further evidenced in the detection of Fe 2p_{3/2} peak (Fig. 20(d)) at binding energies of ≈707 eV and 711 eV, respectively [27,28]. Based on this result, it was thus confirmed that iron sulfide and iron carbonate had precipitated on the steel surface to provide the observed corrosion protection, in spite of the bulk solution been acidic.

5. Conclusions

The addition of H₂S (100 ppm) into CO₂ environments reduced the corrosion rate of carbon steel at pHs 3 and 4 (under-saturated conditions).

The inhibition effect of H₂S on the CO₂ corrosion is attributed to the formation of thin iron sulfide film (tarnish) on the steel surface, which suppressed the anodic dissolution reaction.

The precipitation of iron sulfide and iron carbonate in acidic solution is possible due to local saturation and alkaline conditions on steel surface, and these precipitations provides corrosion protection in the acidic solutions.

References

- [1] M. Bonis, M. Girgis, K. Goerz, R. MacDonald, CORROSION/2006, Paper No. 06122, 2006.
- [2] S.N. Smith, M. Joosten, CORROSION/2006, Paper No. 06115, 2006.
- [3] E.C. Greco, W.B. Wright, Corrosion 18 (1962) 119t.
- [4] J.B. Sardisco, W.B. Wright, E.C. Greco, Corrosion 19 (1963) 354t.
- [5] J.B. Sardisco, R.E. Pitts, Corrosion 21 (1965) 245.
- [6] H. Ma, X. Cheng, G. Li, S. Chen, Z. Quan, S. Zhao, L. Niu, Corros. Sci. 42 (2000) 1669.
- [7] E. Abelev, T.A. Ramanarayanan, S.L. Bernasek, J. Electrochem. Soc. 156 (2009) C331.
- [8] W. Sun, S. Nescic, S. Papavinasan, Corrosion 64 (2008) 586.
- [9] R.A. Berner, Am. J. Sci. 265 (1967) 773.
- [10] P. Taylor, Am. Mineral. 65 (1980) 1026.
- [11] J.S. Smith, J.D.A. Miller, Br. Corros. J. 10 (1975) 136.
- [12] D.W. Shoesmith, P. Taylor, M.G. Bailey, D.G. Owen, J. Electrochem. Soc. 125 (1980) 1007.
- [13] M. Stern, A.L. Geary, J. Electrochem. Soc. 104 (1957) 56.
- [14] S.W. Dean, Handbook on Corrosion Testing and Evaluation, John Wiley, New York, 1971, p. 171.
- [15] E. McCafferty, Corros. Sci. 39 (1997) 243.
- [16] D.D. MacDonald, M.C.H. Mckubre, J.O.M. Bockris, B.E. Conway, R.E. White (Eds.), Modern Aspects of Electrochemistry, vol.14, Plenum Press, New York, 1982, p. 61.
- [17] K.J. Lee, S. Nescic, CORROSION/2006, Paper No. 06417, 2006.
- [18] M. Keddiam, O.R. Mattos, H. Takenouti, J. Electrochem. Soc. 128 (1981) 257.
- [19] M. Keddiam, O.R. Mattos, H. Takenouti, J. Electrochem. Soc. 128 (1981) 266.
- [20] K. Videm, J. Kvarekvål, Corrosion 51 (1995) 260.
- [21] L.G. Benning, R.T. Wilkin, H.L. Barnes, Chemical Geology, 167, 2000, p. 25.
- [22] W. Sun, Ph.D. Diss., Ohio University, 2006.
- [23] W. Sun, S. Nescic, D. Young, R.C. Woollam, Ind. Eng. Chem. Res. 47 (2008) 1738.
- [24] J. Han, B.N. Brown, D. Young, S. Nescic, J. Appl. Electrochem. 40 (2010) 683.
- [25] A. Criaud, C. Fouillac, B. Marty, Geothermics 18 (1989) 711.
- [26] W. Sun, S. Nescic, R.C. Woollam, Corros. Sci. 51 (2009) 1273.
- [27] M. Mullet, S. Boursiquot, M. Abdelmoula, J.-M. Génin, J.-J. Ehrhardt, Geochim. Cosmochim. Acta 66 (2002) 829.
- [28] D.A. Lopez, W.H. Schreiner, S.R. de Sanchez, S.N. Simison, Appl. Surf. Sci. 207 (2003) 69.
- [29] D.A. Lopez, W.H. Schreiner, S.R. de Sanchez, S.N. Simison, Appl. Surf. Sci. 236 (2004) 77.